

Stretchable and self-healable semiconductive composites based on hydrogen bonding-crosslinked elastomeric matrix

Yunfei Wang[‡], Kai-Lin Chen[‡], Nathaniel Prine, Simon Rondeau-Gagné, Yu-Cheng Chiu,^{} and*

Xiaodan Gu^{}*

Y. Wang, N. Prine, Dr. X. Gu

School of Polymer Science and Engineering, Center for Optoelectronic Materials and

Devices, the University of Southern Mississippi, Hattiesburg, MS 39406, USA

E-mail: xiaodan.gu@usm.edu

K.-L. Chen, Dr. Y.-C. Chiu

Department of Chemical Engineering, National Taiwan University of Science and Technology, Taipei 106, Taiwan

E-mail: ycchiu@mail.ntust.edu.tw

Dr. S. Rondeau-Gagné

Department of Chemistry and Biochemistry, Advanced Materials Centre of Research,

University of Windsor, Windsor, Ontario N9B3P4, Canada

[‡]These authors contributed equally to this work.

Keywords: stretchable, self-healable, conjugated polymer/elastomer composites, hydrogen bonding-crosslink

This is the author manuscript accepted for publication and has undergone full peer review but has not been through the copyediting, typesetting, pagination and proofreading process, which may lead to differences between this version and the [Version of Record](#). Please cite this article as [doi: 10.1002/adfm.202303031](https://doi.org/10.1002/adfm.202303031).

This article is protected by copyright. All rights reserved.

Abstract

Semiconductors with both high stretchability and self-healing capability are highly desirable for various wearable devices. Blending conjugated polymers (CPs) with deformable elastomers was a promising method to fabricate stretchable semiconductors due to the wide range of attainable elastic modulus, and deformability. Much progress had been achieved in designing highly stretchable semiconductor polymers or composites. The demonstration of self-healable semiconducting composites is still rare. Here, we developed an extremely soft, highly stretchable, and self-healable hydrogen bonding crosslinked elastomer, amide functionalized-polyisobutylene (PIB-amide), to enable a self-healable semiconductive blend through compounding with a high-performance conjugated diketopyrrolopyrrole (DPP-T) polymer. With the help of a non-covalent hydrogen bonding crosslink, the composite consisting of 20% of the DPP-T and 80% PIB-amide showed record high crack-onset strain (COS ~1500%), extremely low elastic modulus ($E \sim 1.6$ MPa), and unique ability to spontaneously self-heal at the room temperature within 5 mins. Unlike previous works, these unique composite materials also showed strain-independent charge mobility. An in-depth morphological study based on UV-Vis spectroscopy, atomic force microscopy, and X-ray scattering techniques indicated the composites showed blending ratio- and stretching-independent fibril-like aggregation in all composites due to the strong hydrogen bond in elastomer to enable the unique stable charge mobility. This work provides new direction to develop highly healable and electronically stable semiconductive composite and will enable new applications of stretchable electronics.

1. Introduction

Developing stretchable and self-healable semiconductors is very important to meet the growing in the interest of designing wearable and implantable electronics.^[1–8] Conjugated polymers (CPs), due to wide range tunable chemical structures and high flexibility and deformability compared to their inorganic counterpart, are widely adopted in wearable devices, and used as the charge transport layer.^[9–12] Unfortunately, a rigid and coplanar backbone and high crystallinity are preferred to enable effective charge transport for CPs, commonly renders them as rigid and brittle.^[13–15] Therefore, designing CPs with balanced electrical performance and mechanical robustness is required. Besides, mechanical fracture and accidental scratching in long-term use in daily life make the materials less durable.^[8] In this regard, researchers developed a strong interest in making self-healing semiconductors or composite to mitigate above mentioned issues.^[4–7,16]

Most efforts have focused on modifying chemical structures via backbone/side-chain engineering to develop stretchable and self-healable CPs. To improve stretchability, attaching longer and branched alkyl side chains,^[17–21] inserting flexible conjugation breaker spacers^[15,22–28], and copolymerizing soft segments with conjugated polymers^[29–34] are generally used. However, the increased stretchability often resulted in sacrificed charge carrier mobility.^[35] To introduce self-healing ability, dynamic covalent bonds (i.e., Diels-Alder reactions, imine bonds, disulfide exchanges, borate ester bonds) or noncovalent interactions (i.e., hydrogen bonds,^[24,36,37] metal-ligands interaction,^[38] host-guest interactions^[39]) were often incorporated between the polymer chains. Despite considerable progress in developing self-healing polymeric materials,^[40] only a few have focused on electronically active materials and demonstrate their usage in thin-film field-effect transistors. Besides, it must be noted that the molecular design of novel CPs always needs elaborate

synthesis. Due to the conjugated nature of CP's rigid backbone, the demonstration of intrinsically stretchable and room temperature self-healable CPs is still limited.

Alternatively, physical blending CPs with soft elastomers (i.e., polydimethylsiloxane (PDMS),^[41–44] styrene-ethylene-butylene-styrene (SEBS),^[45–48] polystyrene-block-polyisoprene-block-polystyrene (SIS),^[49] rubber,^[50,51] etc.) is a straightforward and effective approach to create stretchable semiconductor.^[44,45,55,46–48,50–54] For example, Bao *et al.* blended SEBS with DPPT-TT fabricating DPPT-TT/SEBS semiconducting composite.^[48] Utilizing the conjugated polymer/elastomer phase separation-induced elasticity (CONPHINE) method, the high charge mobility of $\sim 1 \text{ cm}^2/\text{V s}$ was successfully retained even at 100% strain. Later on, the same group systematically studied the MW influence of both CPs and SEBS on the performance of composites. For CPs with high MW, the aggregation slightly decreased upon increasing MW of SEBS, while opposite trend for CPs with low MW.^[56] Furthermore, they also developed an elastic composite with the help of covalent crosslink between azide and C=C group in SEBS and C-C bond in CPs.^[57] No residual strain showed up with increasing cyclic strains from 10–70%. Jeong *et al.*, first used PDMS as elastomer matrix for the composite. The formation of P3HT bundle network in composite films enable high stretchability of composite (COS>50%).^[46] However, the mobility significantly decreased upon stretching. Cho group embedded P3HT nanowires into PDMS matrix.^[42] The obtaining composites showed stable stretchability at strain up to 100%. Reichmanis group detailed studied processing condition effect on the performance on the P3HT/PDMS composite.^[44] The one with 'predeposition processed' P3HT showed 44 times higher hole mobility than untreated one with high stretchability up to 100% strain. Apart from those previous demonstration of the deformable composite, the self-healable capability for semiconductor composites is rarely demonstrated. Recently, Zhang *et al.* selected butyl rubber, an elastomer with high elasticity and strong adhesion, as the matrix to blend with

DPPTVT.^[50] Although stretchable and self-healing ability was successfully achieved, a mismatch happened between the composite with blending ratio for the highest electrical performance and best mechanical stretchability. Jeong *et al.* embedded Poly(3-butylthiophene-2,5-diyl) (P3BT) nanowires with dopant tris(pentafluorophenyl)borane (BCF) into thermoplastic elastomer matrix SIS fabricating SIS/P3BT/BCF composite. The obtained composites exhibited good thermoelectric performance, achieved self-healing under mild heat and pressure conditions and good stretchability.^[49] Oh, *et al.* fabricated metal-ligands crosslinked DPP-TVT-PDCA/PDMS-PDCA composites.^[58] With the dynamic metal-ligands interaction, the composites showed high stretchability (COS>1300%) and self-healing ability. But the healing rate was relatively low, which needs 1 day to heal fully. Therefore, developing composites with both high stretchability and strong self-healing ability is of great interest to expand the application space for stretchable electronics.

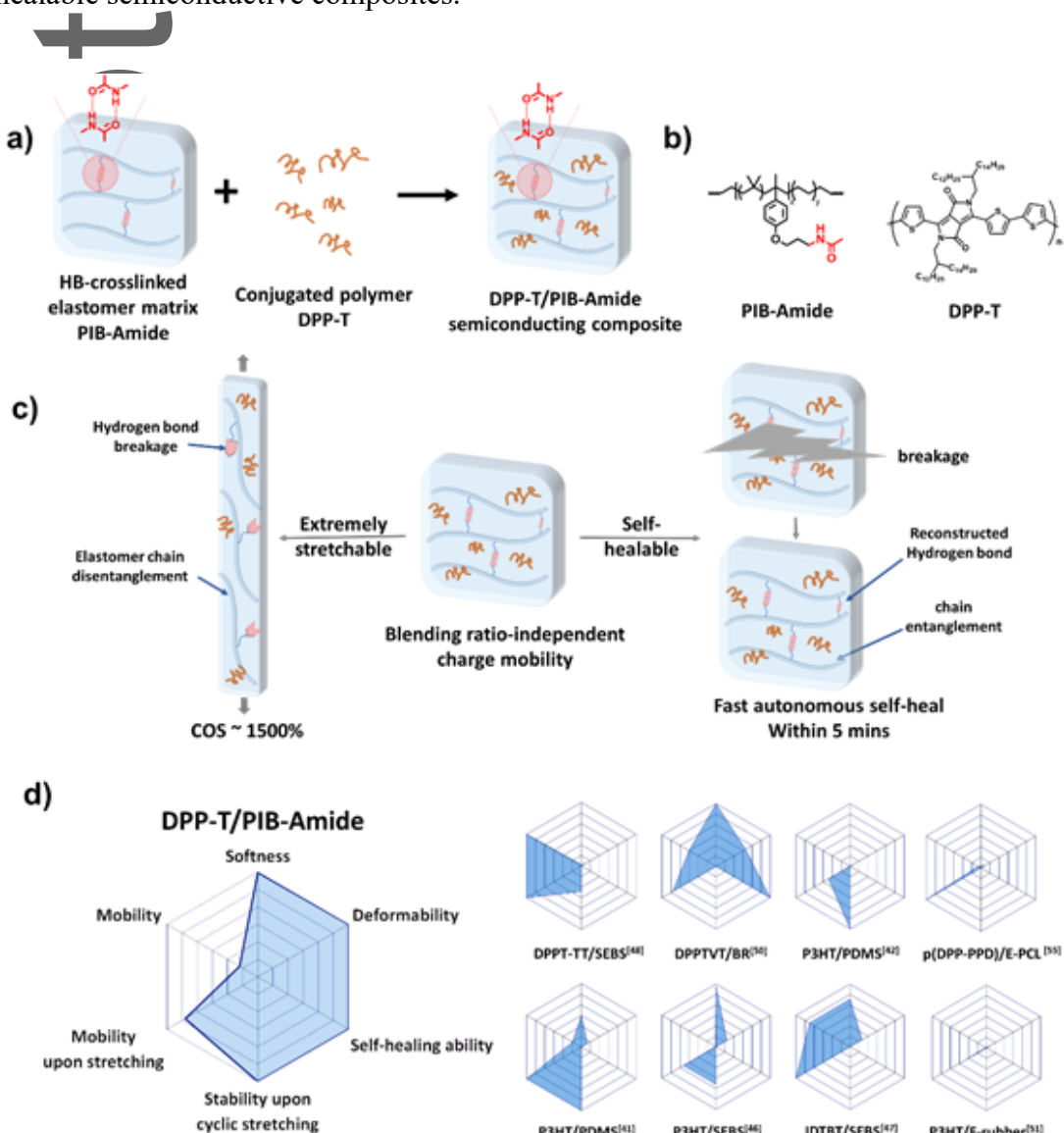
To achieve the above goal, one can resort to the design new high stretchable and self-healable elastomers with the needed properties for the semiconductive polymers. It's reported that polyisobutylene (PIB)-based networks have good flexibility and strong adhesion due to the softness and strong entanglement of the polymer chains.^[59] Along this line, Higashihara incorporated PIB with P3HT synthesizing a block copolymer P3HT-*b*-PIB-*b*-P3HT. With the help of PIB segment, the obtained composite showed high stretchability with COS up to 200%.^[60] Therefore, we expect PIB should own great potential to be used as elastomer matrix to achieve stretchability and self-healing ability.

Introducing hydrogen bond crosslink into elastomers was reported to improve the stretchability and self-healing ability effectively.^[61,62,71,63-70] The weaker dynamic bond is easy to break, providing an extra energy dissipation pathway to improve stretchability. After releasing stretching, the dynamic hydrogen bonds can reconnect again, enabling intrinsically

self-healing ability.^[70] For example, Yan *et al.* utilized the ureidopyrimidinone (UPy) group to successfully construct a hydrogen bonding crosslinked supramolecular polymeric material (SPMs).^[72] With 20 mol% UPy group, an extremely stretchable material (COS= 17,000%) with excellent self-healing ability was obtained. Considering the excellent performance, hydrogen-bonding crosslinked elastomer should be a type of matrix with a high potential for stretchable and self-healable composites. However, far fewer advances have specifically addressed the availability of hydrogen bonding-crosslinked elastomers used in electronics and the influence of hydrogen bond on the performance of semiconducting composites.

Here, we designed a new hydrogen bonding crosslinked amide-functional PIB (PIB-Amide) to enable extremely soft, stretchable, and self-healable semiconductive composites. With PIB-Amide as the elastomer matrix, the semiconducting composite DPP-T/PIB-Amide exhibits blend ratio-independent mobility, with the extreme softness ($E \sim 1.76$ MPa), high stretchability (COS $\sim 1500\%$), and strong self-healing ability at the room temperature (**Scheme 1**). In the meantime, the high charge carrier mobility of our composite can be mainly maintained under 100% cyclic strain for over 100 times. The properties were compared with reported semiconducting composites, which showed impressive improvement (**Scheme 1d**). Wide-angle x-ray scattering (WAXS), polarized UV-vis spectroscopy, and atomic force microscopic combined with infrared-spectroscopy (AFM-IR) were utilized to study the deformation mechanism. Through the in-depth morphology study, we conclude that the deformation happened mostly in the elastomer matrix while the network of the CPs fibril was connected throughout the stretching process, thus allows the composite to maintain stable charge carrier mobility at different strains. This work demonstrated that CP/elastomer composites with hydrogen bonding crosslinked elastomer as the matrix can dramatically increase the stretchability and self-healing ability, which enriches the stretchable

semiconductors materials choice and provides a guideline for the future design of stretchable and healable semiconductive composites.

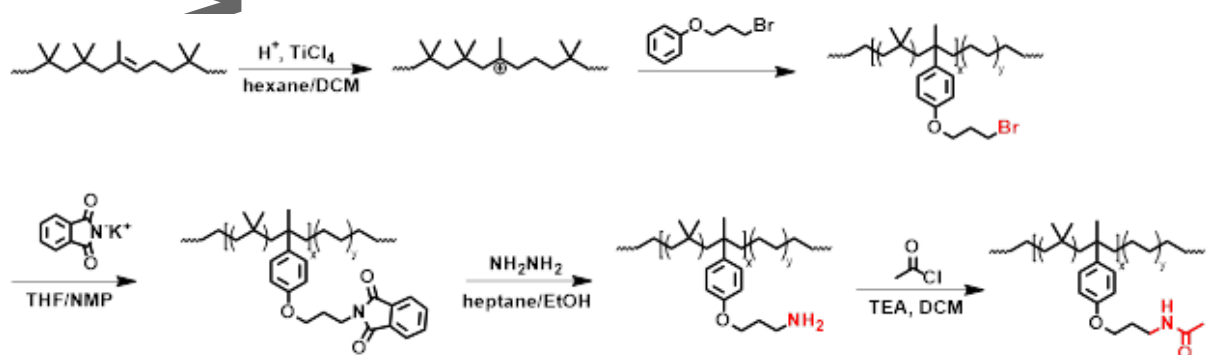


Scheme 1. a) Fabrication of DPP-T/PIB-Amide composite. b) chemical structures of PIB-Amide and DPP-T. c) Schematic diagram showing the stretchable and self-healable DPP-T/PIB-Amide semiconducting composites. d) Comparison of the performance of the current system to previously reported semiconducting conjugated polymer/elastomer composites.

2. Results and Discussion

This article is protected by copyright. All rights reserved.

Scheme 1 showed the overall design strategy of the extremely soft, stretchable, and self-healable semiconductor composites DPP-T/PIB-Amide. In our design, we engineered the non-covalent interactions into the elastomeric matrix. We expect the hydrogen bonding crosslink in elastomer can effectively improve the composite's stretchability, self-healing ability and charge carrier mobility. PIB-Amide was designed as the hydrogen bonding crosslinked elastomer matrix to take advantages of properties of PIB and non-covalent hydrogen bonding crosslink (**Scheme 2**). PIB is a soft and deformable elastomer with strong adhesion. Hydrogen bonding is an effective method to improve stretchability and self-healing ability. Combining these two components, the obtained PIB-Amide enables extreme softness (~ 1 MPa), high stretchability (COS>1600%), and room temperature spontaneous self-healing ability. The detailed synthesis and characterization of PIB-Amide were described in detail in Supporting Information (**Figure S1-7**). DPP-T was selected as the model CP because of the commercial availability and high charge mobility ($\mu \sim 0.2 \text{ cm}^2 \text{ V}^{-1} \text{ s}^{-1}$, **Figure S8-9**).



Scheme 2. Synthetic route of PIB-Amide.

The blending ratio between CPs and elastomers was reported to significantly influence the electrical and mechanical properties of DPP-T/PIB-Amide composites.^[50] We first studied the effect of the blend ratios (weight ratio of DPP-T at 0, 20, 30 and 40% in the

DPP-T/PIB-Amide composites) on their physical and electrical property. This blending ratio range is selected to ensure elastomer forms the matrix or continuous phase (weight ratio of CPs < 50%). A top-contact bottom-gate organic field-effect transistor (OFET) was fabricated to study the electrical properties of DPP-T/PIB-Amide composites (**Figure 1a and S10-11**). A fixed V_{sd} value of -60 V was used for all the transfer curve measurement. Notably, to avoid overestimating the electrical properties, the reliability factor of mobility calculations have substantiated exceeding 90%.^[73] As the result, an average charge carrier mobility around 0.09 $\text{cm}^2 \text{ V}^{-1} \text{ s}^{-1}$ was observed for all 10%-40% DPP-T/PIB-Amide composites, in which 20% DPP-T/PIB-Amide composite showed slightly higher average charge carrier mobility, $\sim 0.15 \text{ cm}^2 \text{ V}^{-1} \text{ s}^{-1}$. This stable charge mobility is attributed to fibril-like chain aggregation, which can exist in composites at different blending ratios, as will be discussed later. Pseudo-free standing tensile test was then performed to evaluate the mechanical properties of composites (**Figure 1b-c, S12, Table S2**).^[74,75] Sample composite film with 13 μm film thickness were prepared. 10% DPP-T/PIB-Amide composite absorbed water strongly, thus the data are not reported here. For the other three composites, 20% DPP-T/PIB-Amide showed a record highest COS of $\sim 1500\%$ while maintaining a low E of 1.65 MPa. As the ratio of DPP-T increased, the COS continuously decreased to $\sim 7.67\%$ (40% DPP-T/PIB-Amide) while E increased to 24.34 MPa, which was still much lower than pure DPP-T (483.62 MPa). Combining the aforementioned results, the blending ratio showed almost no effect on electrical properties but significant influence on mechanical properties. 20% of DPP-T was determined to be the optimum blend ratio due to the highest stretchability and as well as high charge carrier mobility, which was selected for further studies.

Morphology study was then performed to fully elucidate the observed mechanical and electrical properties using infrared-spectroscopy combined atomic force microscopy (AFM-

IR) and grazing-incidence wide-angle x-ray scattering (GIWAXS). To obtain AFM-IR images, FT-IR spectroscopy was first performed on both pure CPs and elastomers to find a non-overlapping absorption peak for both components (**Figure S13**). Comparing the absorption spectra of CPs and PIB-Amide, 1666 cm^{-1} (-C=O stretching vibration in amide) and 1471 cm^{-1} (-CH₂ torsional vibration in backbone) were chosen for selectively excited DPP-T and PIB-Amide, respectively. AFM tapping modes were then applied to obtain phase images (**Figure 1d**). After applying IR mode, two components can be clearly distinguished and here they are labeled with two different colors (**Figure 1e**). The red and green region represent the DPP-T and PIB-Amide, respectively. Both nanoscopic fibril-like aggregation from CPs and macro phase separation between CPs and PIB-Amide were observed for composites with all blending ratios. However, with an increased ratio of DPP-T, the macro-phase separation became more extensive, while fibril-like aggregation remains constant and well dispersed in rubber matrix. We attributed this blending ratio-independent fibril-like aggregation to hydrogen bonding crosslink between PIB. The hydrogen bond limits the chain mobility of elastomer, making the CP chain interact more with each other to form both the fibril and the large aggregation. The aggregation of conjugated polymers was reported beneficial to electrical properties of composites.^[76,77] For example, Lee et al. added DMSO additive into PEDOT:PSS which inducing aggregation of PSS phase.^[77] The aggregation effectively enhanced cohesion and electrical conductivity. Ouyang et al. studied other additives and observed similar phenomenon.^[76] The formation of aggregation and enhanced conductivity was also observed with additive DEG and PEG 400. In terms of charge mobility in OFET applications, previous literature reports fibril-like CP aggregations in CP/elastomer composites contribute mostly.^[78] Therefore, this explains that for four different composites, they all showed similar charge mobility regardless of blending ratios. The morphology for bottom surface of the 20% DPP-T/PIB-Amide composite was also measured using AFM due

to the significance for charge mobility, which showed similar result as top surface (**Figure S14**). On the other hand, macro phase separation would lead to more rigid and brittle DPP phase due to their high modulus and low deformability. Therefore, with increasing mixing ratio of DPP-T in composites, the E increased while deformability decreased. GIWAXS was then performed to study the crystallite structure of DPP-T domain in DPP-T/PIB-Amide composites (**Figure S15-16, Table S3**). Similar value of lamella packing distance and FWHM were obtained, indicating that the blending ratio did not change the crystallite lattice packing, which also further provides insight to support the observed blending ratio-independent charge mobility.

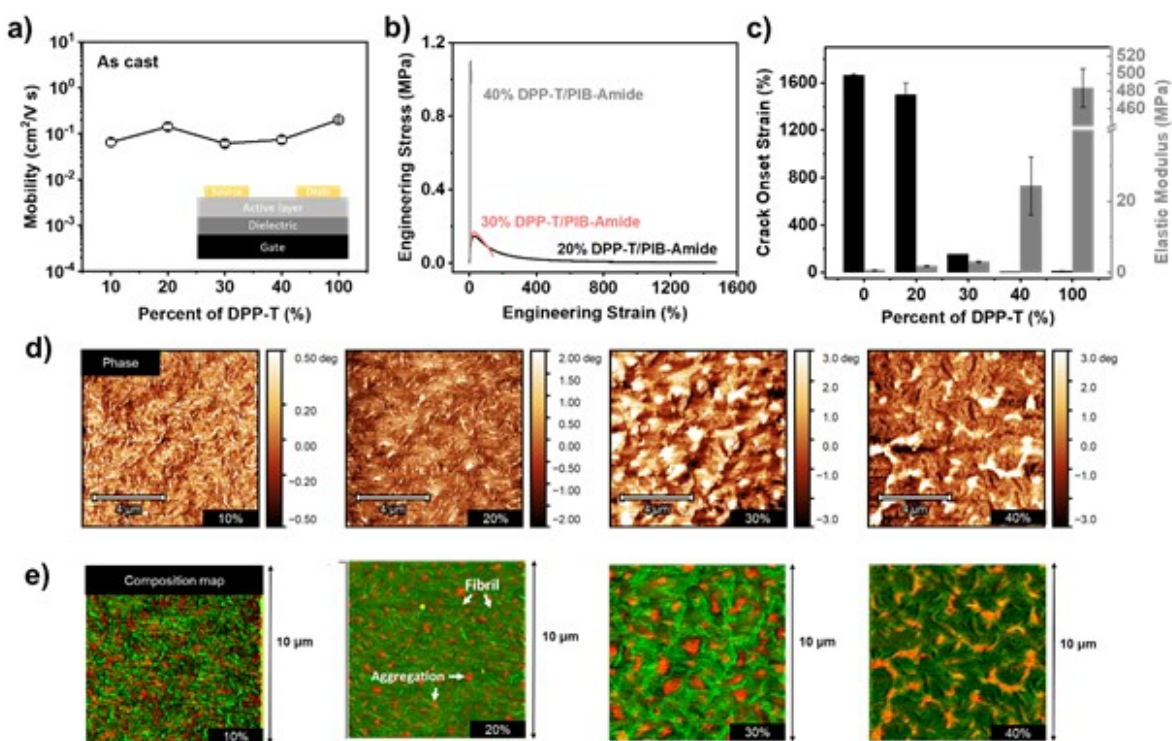


Figure 1. Mechanical, electrical, and morphology for DPP-T/PIB-Amide composite films with different blending ratios. a) Charge carrier mobility of 10-40% DPP-T/PIB-Amide composites and DPP-T thin films from top-contact bottom-gate OFET devices. b) Representative stress-strain curve of 20-40% DPP-T/PIB-Amide composite films. c) Elastic

modulus and crack onset strain of 0, 20-40%, and 100% DPP-T/PIB-Amide composite films.

d) AFM phase images of 10-40% DPP-T/PIB-Amide composite films. e) AFM-IR overlay images highlighting the distributions of DPP-T and PIB-Amide in 10-40% DPP-T/PIB-Amide composite films (red color represents DPP-T domain selectively excited using 1664 cm^{-1} laser, and green color represents for PIB-Amide domain selectively excited using 1462 cm^{-1} laser.

The effect of hydrogen bonding on composites' electrical and mechanical properties was also studied using 20% DPP-T blended with various elastomer control samples (unmodified rubber, intermediate rubber product PIB-Br (**Scheme 2**) which does not have any hydrogen bonding functional group, and hydrogen bonding crosslinked PIB-Amide) (**Figure S17, 18**). The synthesis of the PIB-Br can be found in supporting information as well.^[79] The charge mobility of 20% DPP-T/BR, DPP-T/PIB-Br, and DPP-T/PIB-Amide were investigated. All composites performed similar charge mobilities indicating that the hydrogen bond on elastomer didn't significantly influence the electrical properties (**Figure S17a**). The effect of hydrogen bonds on mechanical properties was studied between 20% DPP-T/PIB-Br and DPP-T/PIB-Amide (**Figure S17b, S18**). The 20% DPP-T/PIB-Br showed COS of 400%, which was much lower than 20% DPP-T/PIB-Amide (COS~1500%), demonstrating hydrogen bonding improved the stretchability of semiconducting composites due to the extra energy dissipation pathway provided by hydrogen bonds. Therefore, hydrogen bonding crosslink between elastomers can effectively improve the deformability of CP/elastomer semiconductor composites while maintaining device performance.

Maintaining electrical properties upon stretching and cyclic stretching plays a vital role in practical use. Next, the device's electronical property under cyclic mechanical stretch

was investigated. The study focused on using 150% strain. The composite sample were deposited onto the crosslinked elastic PDMS substrate. Then the bilayer sample was cyclically stretched using a motorized tensile stage. The charge mobility remains constant upon stretching (Figure 2a, S19-22). Furthermore, high charge mobility value of the semiconductive composite can maintain over 100 repeated stretching cycles to 100% strain at $0.01 \text{ cm}^2 \text{ V}^{-1} \text{ s}^{-1}$ (Figure 2b, S23-24). These results indicate the 20% DPP-T/PIB-Amide composites show high stability upon stretching and cyclic stretching, which is related to the stable crystallite structure as discussed below.

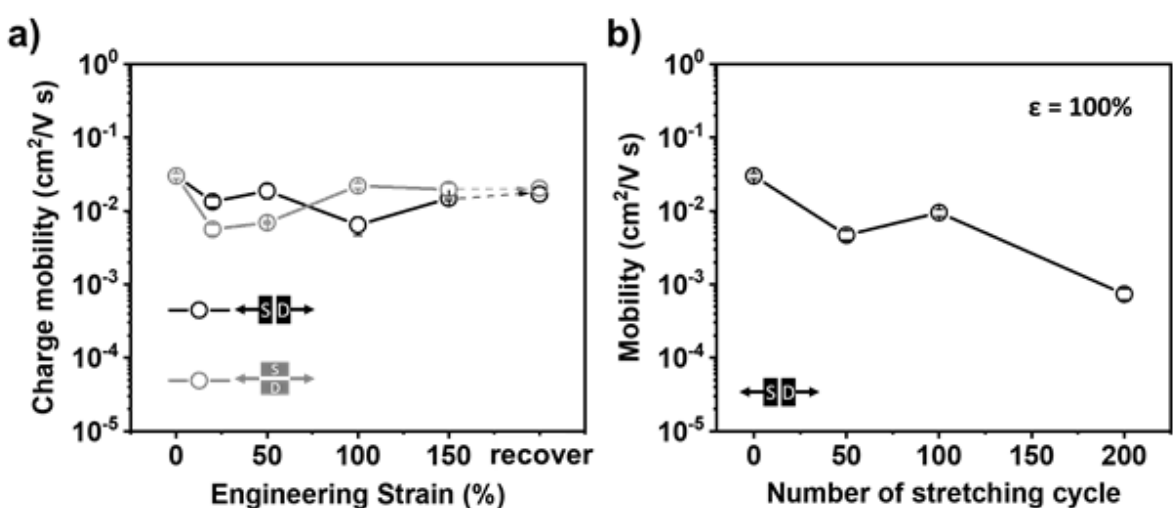


Figure 2. a) Charge carrier mobility of 20% DPP-T/PIB-Amide composites film upon stretching and recovery in parallel and perpendicular direction to charge transfer direction at different strains without annealing. b) Mobilities of 20% DPP-T/PIB-Amide composites film as a function of 100% strain stretching cycles parallel to the charge transport direction.

The deformation mechanism of 20% DPP-T/PIB-Amide composites was performed to understand the stable charge mobility using multi-model characterization, including WAXS, polarized UV-vis absorption spectra, and AFM (Figure 3).^[20] WAXS was first performed to

investigate the crystallite domain alignment of DPP-T upon stretching. 2D scattering pattern and 1d line-cut profiles were shown in **Figure 3a and S25-26a**. From 2D scattering patterns, the (100) peak attributed to the lamellae packing peak was isotropic at the first 150% strain, indicating no obvious crystallite alignment. At 200% strain, the (100) peak began to become slightly anisotropic, demonstrating the crystallite packing direction started to rotate, and align to the stretch direction. Orientation parameter f was calculated based on pole figure analysis of (100) peak to quantify the degree of crystallite alignment (**Figure S26b**).^[20] f showed a slight enhancement of 0.09 at the initial 150% strain and 0.16 at 200% (**Figure 3c**), indicating that the crystallite domain of DPP-T showed little alignment for the first 150% strain and moderate alignment at 200%. Besides, the lamellar packing distance and FWHM was calculated from WAXS of unstretched 20% DPP-T/PIB-Amide thick film (**Table S4**), which was similar to the thin film from GIWAXS indicating the thickness of film didn't significantly influence the morphology. Polarized UV-vis was next to study the whole DPP-T polymer chain alignment. The normalized absorption spectrum for 20% DPP-T/PIB-Amide composite films under strain was plotted in **Figure 3b**, where peaks at \sim 591 nm and \sim 499 nm were assigned to the 0 \rightarrow 0 and 0 \rightarrow 1 peaks, respectively. Orientation parameter f change based on polarized UV-vis was calculated from the dichroic ratio, R , which was given by $f = (R-1)/(R+1)$. Orientation parameter f also slightly increased to 0.08 for 100% strain, which was much lower than the reported pure DPP polymer value ($f = 0.36$ at 100% strain).^[20] Thus, the whole chain of DPP-T also only aligned a little. Combining results from WAXS and polarized UV-vis, we concluded that the high modulus CP component in composites almost didn't contribute to the first 150% strain, which supported the stable charge mobility upon stretching.

The impressive deformability of the semiconductive composite should be related to the soft elastomer domain, which should account for large strain upon stretching. To certify

the contribution of the PIB-Amide component on stretched composites, AFM was performed (Figure 3d, S27). The white region, where there is higher phase shift in the tapping image, represents the softer elastomer phase, whereas the dark brown region represents high modulus DPP-T domains. At the strain of 150%, the white phase, PIB-Amide, and large DPP-T aggregation was stretched. In contrast, the fibril-aggregation remained constant, indicating that the deformation of elastomer and deformation of large DPP-T aggregation contributed most of the first 150% strain, agreed well with the result from WAXS and polarized UV-vis.

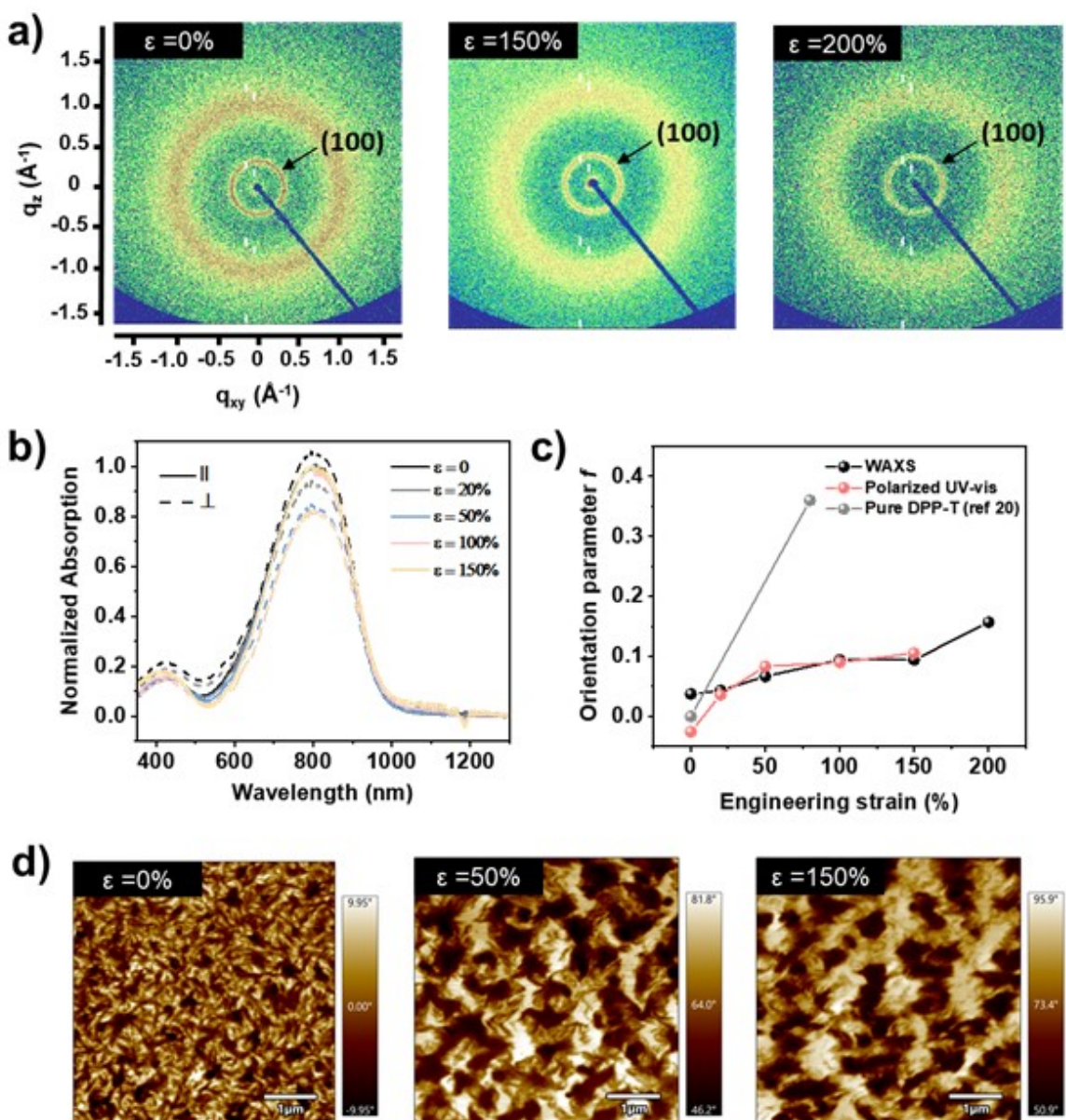


Figure 3. Deformation mechanism of 20% DPP-T/PIB-Amide. a) 2D scattering patterns of stretched 20% DPP-T/PIB-Amide composite films at 0, 150 and 200% strain from WAXS. b) Polarized UV-vis absorption plot of 20% DPP-T/PIB-Amide composite films at 0, 20, 50, 100, and 150 % strain. c) Herman's orientation parameter f versus strain based on WAXS and polarized UV-vis. D) AFM phase images of stretched 20% DPP-T/PIB-Amide composite films at 0, 50, and 150% strains.

Self-healing ability is an important property allowing for repair local defect under cyclic mechanic stress for wearable device in real life scenario. Due to the self-healing ability of PIB-Amide, we expected the DPP-T/PIB-Amide composites should also perform strong self-healing ability. The self-healing ability of 20% DPP-T/PIB-Amide composites was evaluated in two different methods, named ‘scratching film test’ and ‘cutting film healing test’ here respectively. The scratching film method was first performed. In detail, a thick composite film was drop-casted onto a flat silicon wafer and scratched using a razor blade to introduce a scratch into the film (**Figure 4a**). The scratched composites were placed in an air environment without any additional thermal or solvent vapor treatment. To evaluate the self-healing ability, the gap change was monitored using both optical microscopy (OM) and profilometer from 0 to 30 min after scratching (**Figure 4a**). The gap is quickly healed from OM images, where the scratch becomes lighter in color after 5 mins and almost disappeared after 30 mins. The thickness change of the gap was measured by profilometer to quantify the healing processing (**Figure 4b**). After scratching, a ~ 1.5 μm crack was generated and became lighter and lighter within 30 min (~ 1 μm for 8 min, 0.5 μm for 15 min and 0.1 μm for 30 min). Tensile test was then performed to calculate the self-healing efficiency, given by the ratio of COS after self-healing and COS of unscratched composite films.^[80] In 5 mins, the

self-healing efficiency of 20% DPP-T/PIB-Amide composite reached 94% and 100% after 15 mins (**Figure 4c**). Therefore, the 20% DPP-T/PIB-Amide composite showed excellent self-healing ability. To demonstrate the mechanism of self-heal of 20% DPP-T/PIB-Amide composite, the self-healing efficiency of a control sample using non-hydrogen bonding crosslink composite (20% DPP-T/PIB-Br) was also measured (**Figure 4c**). The self-healing efficiency of DPP-T/PIB-Br composite film was 10% for 5 mins and increased to 56% at 30 mins indicating PIB itself has some healing ability due to the low glass transition temperature to promote local chain diffusion and chain entanglement. However, such capability is not on par with the composite using rubber matrix with hydrogen bonding crosslink, where the self-healing ability improved significantly. Therefore, the strong self-healing ability of 20% DPP-T/PIB-Amide composite is attributed to both the association effect of entanglement of PIB chains and hydrogen bonding crosslink. AFM was used to study morphology on the healed part. The healed film showed similar morphology but larger phase separation (**Figure 4d**).

The cutting film method is another method we used here to demonstrate the self-healing ability. Bulk composite films were first drop-cast on Si wafers. After immersing in liquid nitrogen, the bulk film was cut into two separate pieces. The separated pieces were pressed again for 25 seconds, followed by being stretched (See supporting **Movie S2**). The two parts successfully stuck and showed high stretchability indicating the self-healing of DPP-T/PIB-Amide composites were very fast and strong (**Figure 4e**).

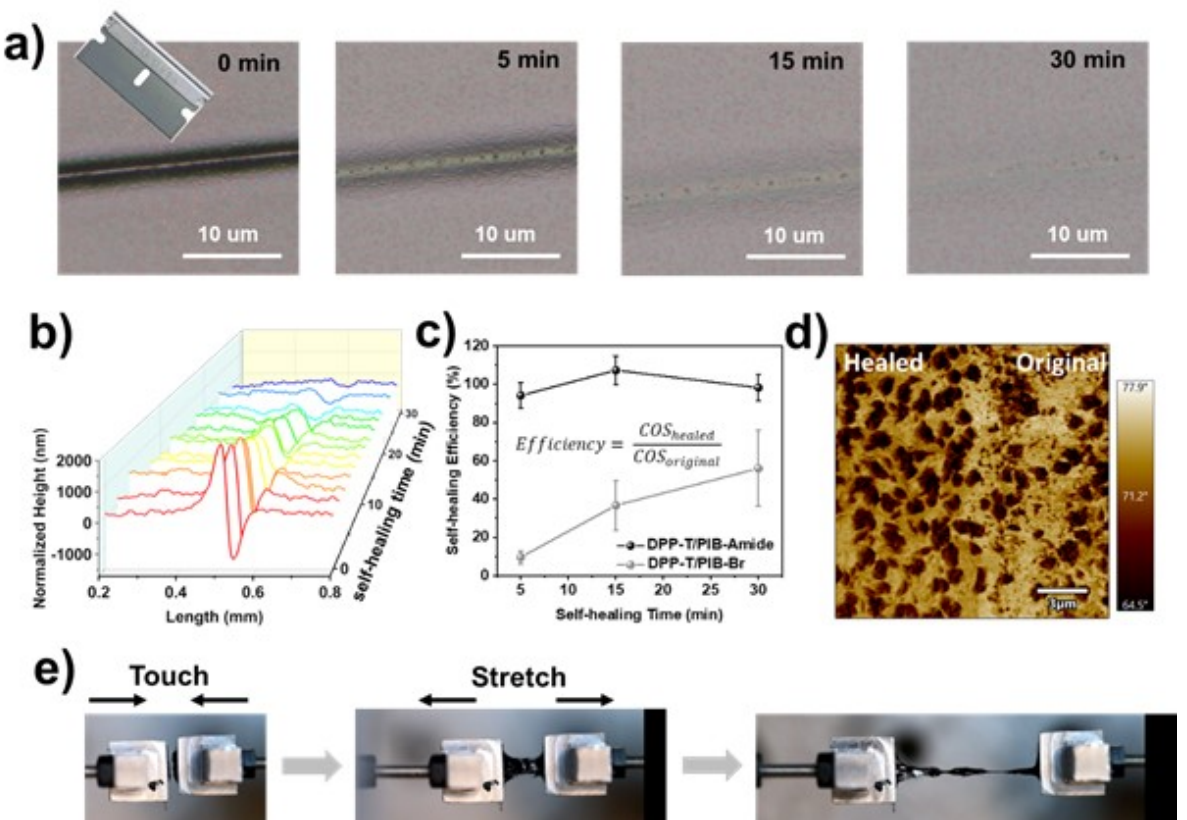


Figure 4. Self-healing ability of 20% DPP-T/PIB-Amide composite films. a) Optical microscope (OM) images of scratched semiconducting film through a self-healing process. b) Thickness map of scratched composite films through the self-healing process. c) Self-healing efficiency through the self-healing process. d) AFM phase images of healed composite films. e) Photographs of the self-healing process of composites from ‘cutting film’ method.

3. Conclusion

In summary, we successfully synthesized hydrogen bonding crosslinked elastomer, PIB-Amide, to fabricate a CP/elastomer composite with record highest crack-onset strain of 1500%, the low elastic modulus of 1.6 MPa, blending ratio-independent charge mobility of $\sim 0.09 \text{ cm}^2 \text{ V}^{-1} \text{ s}^{-1}$ and stable electrical property upon cyclic stretching. Morphology study indicated the elastomer domain accommodated most of the strain upon stretching, allow the

electronic active conjugated polymer fibril phase to remain intact, allow maintaining a high and stable charge carrier mobility. The strong self-healing ability originates from the association effect of chain entanglement of PIB and the dynamic nature of hydrogen bonds. This work developed a new semiconducting composite with all-around high performance, which enriches the stretchable semiconducting polymer and provides a guideline for the future design of stretchable semiconductors.

Supporting Information

Supporting Information is available from the Wiley Online Library or from the author.

Acknowledgement

We thank National Science Foundation under ward number DMR-2047689 for supporting this work. S.R.-G. thank the Natural Sciences and Engineering Research Council of Canada (NSERC) for financial support through a Discover Grant (RGPIN-2022-04428). K.-L. C. and Y.-C. C. thank the financial support from the Ministry of Science and Technology in Taiwan (MOST 111-2628-E-011-008-MY3). Work at the Molecular Foundry was supported by the Office of Science, Office of Basic Energy Sciences, of the U.S. Department of Energy under Contract No. DE-AC02-05CH11231. The authors thank Chih-Ting Liu and Dr. Lifeng Huang for assistance of device performance, Dr. Kyle Mehringer, Logan Dugas, Dana Pinson and Dr. Robson Storey for help of synthesis of rubbery materials, Dr. Haoyu Zhao, Dr. Zhiqiang Cao, Dr. Song Zhang and Dr. Luke A. Galuska for suggestions of morphology characterization.

Received: ((will be filled in by the editorial staff))

Revised: ((will be filled in by the editorial staff))

Published online: ((will be filled in by the editorial staff))

References

- [1] D. H. Kim, N. Lu, R. Ma, Y. S. Kim, R. H. Kim, S. Wang, J. Wu, S. M. Won, H. Tao, A. Islam, K. J. Yu, T. Il Kim, R. Chowdhury, M. Ying, L. Xu, M. Li, H. J. Chung, H. Keum, M. McCormick, P. Liu, Y. W. Zhang, F. G. Omenetto, Y. Huang, T. Coleman, J. A. Rogers, *Science*. **2011**, *333*, 838.
- [2] D. J. Lipomi, Z. Bao, *MRS Bull.* **2017**, *42*, 93.
- [3] D. Son, J. Lee, S. Qiao, R. Ghaffari, J. Kim, J. E. Lee, C. Song, S. J. Kim, D. J. Lee, S. W. Jun, S. Yang, M. Park, J. Shin, K. Do, M. Lee, K. Kang, C. S. Hwang, N. Lu, T. Hyeon, D. H. Kim, *Nat. Nanotechnol.* **2014**, *9*, 397.
- [4] Z. Ma, H. Li, X. Jing, Y. Liu, H. Y. Mi, *Sensors Actuators, A Phys.* **2021**, *329*, 112800.
- [5] S. Latif, S. Amin, S. S. Haroon, I. A. Sajjad, *Mater. Res. Express* **2019**, *6*.
- [6] H. Yue, Z. Wang, Y. Zhen, *ACS Omega* **2022**, *7*, 18197.
- [7] F. Mashkoor, S. J. Lee, H. Yi, S. M. Noh, C. Jeong, *Int. J. Mol. Sci.* **2022**, *23*, 1.
- [8] L. Laysandra, A. Njotoprajitno, S. P. Prakoso, Y. C. Chiu, *Mater. Adv.* **2022**, *3*, 7154.
- [9] K. Müllen, W. Pisula, *J. Am. Chem. Soc.* **2015**, *137*, 9503.
- [10] S. Himmelberger, A. Salleo, *MRS Commun.* **2015**, *5*, 383.
- [11] C. B. Nielsen, M. Turbiez, I. McCulloch, *Adv. Mater.* **2013**, *25*, 1859.

This article is protected by copyright. All rights reserved.

[12] H. N. Tsao, K. Müllen, *Chem. Soc. Rev.* **2010**, *39*, 2372.

[13] R. Noriega, J. Rivnay, K. Vandewal, F. P. V. Koch, N. Stingelin, P. Smith, M. F. Toney, A. Salleo, *Nat. Mater.* **2013**, *12*, 1038.

[14] H. Sirringhaus, M. Bird, T. Richards, N. Zhao, *Adv. Mater.* **2010**, *22*, 3893.

[15] S. E. Root, S. Savagatrup, A. D. Printz, D. Rodriquez, D. J. Lipomi, *Chem. Rev.* **2017**, *117*, 6467.

[16] J. Kang, J. B. H. Tok, Z. Bao, *Nat. Electron.* **2019**, *2*, 144.

[17] D. Liu, J. Mun, G. Chen, N. J. Schuster, W. Wang, Y. Zheng, S. Nikzad, J. C. Lai, Y. Wu, D. Zhong, Y. Lin, Y. Lei, Y. Chen, S. Gam, J. W. Chung, Y. Yun, J. B. H. Tok, Z. Bao, *J. Am. Chem. Soc.* **2021**, *143*, 11679.

[18] F. Sugiyama, A. T. Kleinschmidt, L. V. Kayser, D. Rodriquez, M. Finn, M. A. Alkhadra, J. M. H. Wan, J. Ramírez, A. S. C. Chiang, S. E. Root, S. Savagatrup, D. J. Lipomi, *Polym. Chem.* **2018**, *9*, 4354.

[19] H.-C. Yen, Y.-C. Lin, W.-C. Chen, *Macromolecules* **2021**, *54*, 1665.

[20] S. Zhang, A. Alesadi, G. T. Mason, K. L. Chen, G. Freychet, L. Galuska, Y. H. Cheng, P. B. J. St. Onge, M. U. Ocheje, G. Ma, Z. Qian, S. Dhakal, Z. Ahmad, C. Wang, Y. C. Chiu, S. Rondeau-Gagné, W. Xia, X. Gu, *Adv. Funct. Mater.* **2021**, *31*, 2100161.

[21] Y. C. Chiang, H. C. Wu, H. F. Wen, C. C. Hung, C. W. Hong, C. C. Kuo, T. Higashihara, W. C. Chen, *Macromolecules* **2019**, *52*, 4393.

[22] J. Mun, G. J. N. Wang, J. Y. Oh, T. Katsumata, F. L. Lee, J. Kang, H. C. Wu, F. Lissel, S. Rondeau-Gagné, J. B. H. Tok, Z. Bao, *Adv. Funct. Mater.* **2018**, *28*,

1804222.

[23] S. Savagatrup, X. Zhao, E. Chan, J. Mei, D. J. Lipomi, *Macromol. Rapid Commun.* **2016**, *37*, 1623.

[24] J. Y. Oh, S. Rondeau-Gagné, Y. C. Chiu, A. Chortos, F. Lissel, G. J. N. Wang, B. C. Schroeder, T. Kurosawa, J. Lopez, T. Katsumata, J. Xu, C. Zhu, X. Gu, W. G. Bae, Y. Kim, L. Jin, J. W. Chung, J. B. H. Tok, Z. Bao, *Nature* **2016**, *539*, 411.

[25] Y. Zheng, M. Ashizawa, S. Zhang, J. Kang, S. Nikzad, Z. Yu, Y. Ochiai, H. C. Wu, H. Tran, J. Mun, Y. Q. Zheng, J. B. H. Tok, X. Gu, Z. Bao, *Chem. Mater.* **2020**, *32*, 5700.

[26] Y. Zhao, X. Zhao, Y. Zang, C. A. Di, Y. Diao, J. Mei, *Macromolecules* **2015**, *48*, 2048.

[27] X. Zhao, Y. Zhao, Q. Ge, K. Butrouna, Y. Diao, K. R. Graham, J. Mei, *Macromolecules* **2016**, *49*, 2601.

[28] Y. Zhao, X. Zhao, M. Roders, A. Gumyusenge, A. L. Ayzner, J. Mei, *Adv. Mater.* **2017**, *29*, 1605056.

[29] C. Müller, S. Goffri, D. W. Breiby, J. W. Andreasen, H. D. Chanzy, R. A. J. Janssen, M. M. Nielsen, C. P. Radano, H. Sirringhaus, P. Smith, N. Stingelin-Stutzmann, *Adv. Funct. Mater.* **2007**, *17*, 2674.

[30] K. Ditte, J. Perez, S. Chae, M. Hambach, M. Al-Hussein, H. Komber, P. Formanek, S. C. B. Mannsfeld, A. Fery, A. Kiriy, F. Lissel, *Adv. Mater.* **2021**, *33*, 2005416.

[31] S. Zhang, M. U. Ocheje, L. Huang, L. Galuska, Z. Cao, S. Luo, Y. Cheng, D. Ehlenberg, R. B. Goodman, D. Zhou, Y. Liu, Y. Chiu, J. D. Azoulay, S. Rondeau-Gagné, X. Gu, *Adv. Electron. Mater.* **2019**, *5*, 1800899.

[32] K. Sato, Y. Hemmi, A. Kato, H. Matsui, K. Fuchise, T. Higashihara, *Polymer (Guildf).* **2022**, *252*, 124934.

[33] R. Peng, B. Pang, D. Hu, M. Chen, G. Zhang, X. Wang, H. Lu, K. Cho, L. Qiu, *J. Mater. Chem. C* **2015**, *3*, 3599.

[34] L. C. Hsu, S. Kobayashi, T. Isono, Y. C. Chiang, B. J. Ree, T. Satoh, W. C. Chen, *Macromolecules* **2020**, *53*, 7496.

[35] A. D. Printz, D. J. Lipomi, *Appl. Phys. Rev.* **2016**, *3*.

[36] M. Y. Lee, S. Dharmapurikar, S. J. Lee, Y. Cho, C. Yang, J. H. Oh, *Chem. Mater.* **2020**, *32*, 1914.

[37] X. Yu, C. Li, C. Gao, X. Zhang, G. Zhang, D. Zhang, *SmartMat* **2021**, *2*, 347.

[38] C. H. Li, C. Wang, C. Keplinger, J. L. Zuo, L. Jin, Y. Sun, P. Zheng, Y. Cao, F. Lissel, C. Linder, X. Z. You, Z. Bao, *Nat. Chem.* **2016**, *8*, 618.

[39] R. Yu, Y. Yang, J. He, M. Li, B. Guo, *Chem. Eng. J.* **2021**, *417*, 128278.

[40] J. H. Xu, C. Di Ding, P. Chen, L. H. Tan, C. B. Chen, J. J. Fu, *Appl. Phys. Rev.* **2020**, *7*.

[41] G. Zhang, S. Lee, E. Gutiérrez-Meza, C. Buckley, M. McBride, D. A. Valverde-Chávez, Y. H. Kwon, V. Savikhin, H. Xiong, T. J. Dunn, M. F. Toney, Z. Yuan, C. Silva, E. Reichmanis, *Chem. Mater.* **2019**, *31*, 6530.

[42] E. Song, B. Kang, H. H. Choi, D. H. Sin, H. Lee, W. H. Lee, K. Cho, *Adv. Electron. Mater.* **2016**, *2*, 1500250.

[43] G. Zhang, M. McBride, N. Persson, S. Lee, T. J. Dunn, M. F. Toney, Z. Yuan, Y. H.

Kwon, P. H. Chu, B. Ristein, E. Reichmanis, *Chem. Mater.* **2017**, *29*, 7645.

[44] D. Choi, H. Kim, N. Persson, P. H. Chu, M. Chang, J. H. Kang, S. Graham, E. Reichmanis, *Chem. Mater.* **2016**, *28*, 1196.

[45] S. Nikzad, H. C. Wu, J. Kim, C. M. Mahoney, J. R. Matthews, W. Niu, Y. Li, H. Wang, W. C. Chen, M. F. Toney, M. He, Z. Bao, *Chem. Mater.* **2020**, *32*, 897.

[46] M. Shin, J. Y. Oh, K. E. Byun, Y. J. Lee, B. Kim, H. K. Baik, J. J. Park, U. Jeong, *Adv. Mater.* **2015**, *27*, 1255.

[47] D. Liu, Z. Ding, Y. Wu, S. F. Liu, Y. Han, K. Zhao, *Macromolecules* **2022**, *55*, 297.

[48] J. Xu, S. Wang, G. J. N. Wang, C. Zhu, S. Luo, L. Jin, X. Gu, S. Chen, V. R. Feig, J. W. F. To, S. Rondeau-Gagné, J. Park, B. C. Schroeder, C. Lu, J. Y. Oh, Y. Wang, Y. H. Kim, H. Yan, R. Sinclair, D. Zhou, G. Xue, B. Murmann, C. Linder, W. Cai, J. B. H. Tok, J. W. Chung, Z. Bao, *Science (80-.)* **2017**, *355*, 59.

[49] Y. J. Jeong, J. Jung, E. H. Suh, D. J. Yun, J. G. Oh, J. Jang, *Adv. Funct. Mater.* **2020**, *30*.

[50] S. Zhang, Y. Cheng, L. Galuska, A. Roy, M. Lorenz, B. Chen, S. Luo, Y. Li, C. Hung, Z. Qian, P. B. J. St. Onge, G. T. Mason, L. Cowen, D. Zhou, S. I. Nazarenko, R. F. Storey, B. C. Schroeder, S. Rondeau-Gagné, Y. Chiu, X. Gu, *Adv. Funct. Mater.* **2020**, *30*, 2000663.

[51] Y. C. Chiang, C. C. Shih, S. H. Tung, W. C. Chen, *Polymer (Guildf.)* **2018**, *155*, 146.

[52] P. Kulatunga, N. Yousefi, S. Rondeau-Gagné, *Chemosensors* **2022**, *10*, 201.

[53] L. Janasz, M. Borkowski, P. W. M. Blom, T. Marszalek, W. Pisula, *Adv. Funct. Mater.*

2022, **32**, 2105456.

[54] S. Riera-Galindo, F. Leonardi, R. Pfattner, M. Mas-Torrent, *Adv. Mater. Technol.* **2019**, **4**, 1900104.

[55] H. Tran, V. R. Feig, K. Liu, H. C. Wu, R. Chen, J. Xu, K. Deisseroth, Z. Bao, *ACS Cent. Sci.* **2019**, **5**, 1884.

[56] A. Peña-Alcántara, S. Nikzad, L. Michalek, N. Prine, Y. Wang, H. Gong, E. Ponte, S. Schneider, Y. Wu, S. E. Root, M. He, J. B. H. Tok, X. Gu, Z. Bao, *Adv. Electron. Mater.* **2023**, 2201055.

[57] Y. Zheng, Z. Yu, S. Zhang, X. Kong, W. Michaels, W. Wang, G. Chen, D. Liu, J. C. Lai, N. Prine, W. Zhang, S. Nikzad, C. B. Cooper, D. Zhong, J. Mun, Z. Zhang, J. Kang, J. B. H. Tok, I. McCulloch, J. Qin, X. Gu, Z. Bao, *Nat. Commun.* **2021**, **12**, 1.

[58] J. Y. Oh, D. Son, T. Katsumata, Y. Lee, Y. Kim, J. Lopez, H. C. Wu, J. Kang, J. Park, X. Gu, J. Mun, N. G. J. Wang, Y. Yin, W. Cai, Y. Yun, J. B. H. Tok, Z. Bao, *Sci. Adv.* **2019**, **5**.

[59] M. Bag, S. Banerjee, R. Faust, D. Venkataraman, *Sol. Energy Mater. Sol. Cells* **2016**, **145**, 418.

[60] T. Higashihara, S. Fukuta, Y. Ochiai, T. Sekine, K. Chino, T. Koganezawa, I. Osaka, *ACS Appl. Polym. Mater.* **2019**, **1**, 315.

[61] G. Tillet, B. Boutevin, B. Ameduri, *Prog. Polym. Sci.* **2011**, **36**, 191.

[62] S. Mavila, O. Eivgi, I. Berkovich, N. G. Lemcoff, *Chem. Rev.* **2016**, **116**, 878.

[63] K. P. Nair, V. Breedveld, M. Weck, *Macromolecules* **2008**, **41**, 3429.

[64] Y. Osada, J.-P. Gong, *Adv. Mater.* **1998**, *10*, 827.

[65] L. R. Rieth, R. F. Eaton, G. W. Coates, *Angew. Chemie Int. Ed.* **2001**, *40*, 2153.

[66] P. Song, H. Wang, *Adv. Mater.* **2020**, *32*, 1901244.

[67] K. E. Feldman, M. J. Kade, E. W. Meijer, C. J. Hawker, E. J. Kramer, *Macromolecules* **2010**, *43*, 5121.

[68] M. C. Stuparu, A. Khan, C. J. Hawker, *Polym. Chem.* **2012**, *3*, 3033.

[69] M. U. Ocheje, B. P. Charron, Y. H. Cheng, C. H. Chuang, A. Soldera, Y. C. Chiu, S. Rondeau-Gagné, *Macromolecules* **2018**, *51*, 1336.

[70] J. A. Neal, D. Mozhdehi, Z. Guan, *J. Am. Chem. Soc.* **2015**, *137*, 4846.

[71] R. J. Wojtecki, M. A. Meador, S. J. Rowan, *Nat. Mater.* **2011**, *10*, 14.

[72] X. Yan, Z. Liu, Q. Zhang, J. Lopez, H. Wang, H. C. Wu, S. Niu, H. Yan, S. Wang, T. Lei, J. Li, D. Qi, P. Huang, J. Huang, Y. Zhang, Y. Wang, G. Li, J. B. H. Tok, X. Chen, Z. Bao, *J. Am. Chem. Soc.* **2018**, *140*, 5280.

[73] H. H. Choi, K. Cho, C. D. Frisbie, H. Sirringhaus, V. Podzorov, *Nat. Mater.* **2017**, *17*, 2.

[74] S. Zhang, L. A. Galuska, X. Gu, *J. Polym. Sci.* **2022**, *60*, 1108.

[75] S. Zhang, M. U. Ocheje, S. Luo, D. Ehlenberg, B. Appleby, D. Weller, D. Zhou, S. Rondeau-Gagné, X. Gu, *Macromol. Rapid Commun.* **2018**, *39*, 1800092.

[76] L. Ouyang, C. Musumeci, M. J. Jafari, T. Ederth, O. Inganäs, *ACS Appl. Mater. Interfaces* **2015**, *7*, 19764.

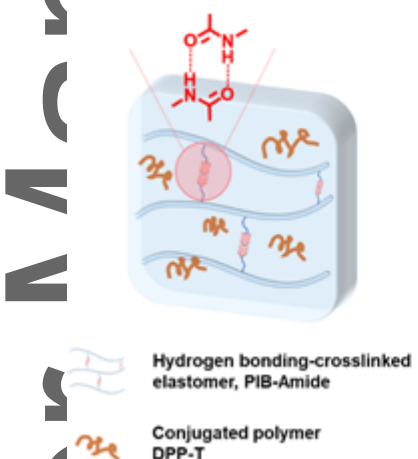
[77] I. Lee, G. W. Kim, M. Yang, T. S. Kim, *ACS Appl. Mater. Interfaces* **2016**, *8*, 302.

[78] I. Angunawela, M. M. Nahid, M. Ghasemi, A. Amassian, H. Ade, A. Gadisa, *ACS Appl. Mater. Interfaces* **2020**, *12*, 26239.

[79] C. G. Campbell, R. F. Storey, *J. Polym. Sci. Part A Polym. Chem.* **2017**, *55*, 1991.

[80] Y. L. Rao, A. Chortos, R. Pfattner, F. Lissel, Y. C. Chiu, V. Feig, J. Xu, T. Kurosawa, X. Gu, C. Wang, M. He, J. W. Chung, Z. Bao, *J. Am. Chem. Soc.* **2016**, *138*, 6020.

Table of contents



- **Extremely stretchable**
COS ~ 1500%
- **Stable charge mobility**
blending ratio independent
stable upon 150% strain
stable upon 100% strain for 100 cycles
- **Fast autonomous self-heal**
within 5 mins

An extremely soft, stretchable, and self-healable conjugated polymer/elastomer semiconductive composite is developed through compounding hydrogen bonding crosslinked elastomer, amide functionalized-polyisobutylene (PIB-amide), with a high-performance conjugated diketopyrrolopyrrole (DPP-T) polymer.